A&A 518, L152 (2010)
DOI: 10.1051/0004-6361/201014600

Herschel: the first science highlights

Astronomy & Astrophysics
Special feature

Letter to the Editor

First results of *Herschel*-PACS observations of Neptune⋆

E. Lellouch[1], P. Hartogh[2], H. Feuchtgruber[3], B. Vandenbussche[4], T. de Graauw[5], R. Moreno[1], C. Jarchow[2], T. Cavalié[2], G. Orton[6], M. Banaszkiewicz[7], M. I. Blecka[7], D. Bockelée-Morvan[1], J. Crovisier[1], T. Encrenaz[1], T. Fulton[8], M. Küppers[9], L. M. Lara[10], D. C. Lis[11], A. S. Medvedev[2], M. Rengel[2], H. Sagawa[2], B. Swinyard[12], S. Szutowicz[7], F. Bensch[13], E. Bergin[14], F. Billebaud[15], N. Biver[1], G. A. Blake[6], J. A. D. L. Blommaert[4], J. Cernicharo[16], R. Courtin[1], G. R. Davis[17], L. Decin[4], P. Encrenaz[18], A. Gonzalez[2], E. Jehin[19], M. Kidger[20], D. Naylor[21], G. Portyankina[22], R. Schieder[23], S. Sidher[12], N. Thomas[22], M. de Val-Borro[2], E. Verdugo[20], C. Waelkens[4], H. Walker[12], H. Aarts[5], C. Comito[24], J. H. Kawamura[6], A. Maestrini[18], T. Peacocke[25], R. Teipen[23], T. Tils[23], and K. Wildeman[5]

(Affiliations can be found after the references)

Received 31 March 2010 / Accepted 14 May 2010

ABSTRACT

We report on the initial analysis of a *Herschel*-PACS full range spectrum of Neptune, covering the 51–220 μm range with a mean resolving power of ~3000, and complemented by a dedicated observation of CH_4 at 120 μm. Numerous spectral features due to HD (R(0) and R(1)), H_2O, CH_4, and CO are present, but so far no new species have been found. Our results indicate that (i) Neptune's mean thermal profile is warmer by ~3 K than inferred from the *Voyager* radio-occultation; (ii) the D/H mixing ratio is $(4.5 \pm 1) \times 10^{-5}$, confirming the enrichment of Neptune in deuterium over the protosolar value ($\sim 2.1 \times 10^{-5}$); (iii) the CH_4 mixing ratio in the mid stratosphere is $(1.5 \pm 0.2) \times 10^{-3}$, and CH_4 appears to decrease in the lower stratosphere at a rate consistent with local saturation, in agreement with the scenario of CH_4 stratospheric injection from Neptune's warm south polar region; (iv) the H_2O stratospheric column is $(2.1 \pm 0.5) \times 10^{14}$ cm^{-2} but its vertical distribution is still to be determined, so the H_2O external flux remains uncertain by over an order of magnitude; and (v) the CO stratospheric abundance is about twice the tropospheric value, confirming the dual origin of CO suspected from ground-based millimeter/submillimeter observations.

Key words. planets and satellites: atmospheres – planets and satellites: individual: Neptune – planets and satellites: composition – techniques: spectroscopic

1. Introduction

Neptune's thermal emission has been initally explored from the ground in the 8–13 μm window and in the millimeter range and by the *Voyager* spacecraft in 1989, but detailed views of its spectrum had to await sensitive instrumentation onboard ISO (see review in Bézard et al. 1999a), *Spitzer* (Meadows et al. 2008) and recently AKARI (Fletcher et al. 2010). Altogether, these observations have revealed a surprisingly rich composition of Neptune's stratosphere, including numerous hydrocarbons (CH_4, C_2H_2, C_2H_6, CH_3, C_2H_4, CH_3C_2H, C_4H_2), oxygen-bearing species (CO, CO_2, and H_2O), HCN, as well as deuterium species CH_3D and HD. Favorable factors for observing minor species in Neptune's atmosphere are (i) its relatively warm stratosphere (~140 K at 1 mbar) that enhances IR emission; and (ii) Neptune's large internal heat source that results in rapid convection updrafting minor disequilibrium species, notably CO, up to observable levels. Neptune's submillimeter spectrum longwards of 50 μm has been observed by ISO/LWS (Burgdorf et al. 2003), but the signal-to-noise ratio in the data was not high enough to reveal spectral features. In this paper, we report the first results from observations of Neptune at 51–220 μm (195–45 cm^{-1}) with the PACS instrument onboard *Herschel* (Pilbratt et al. 2010), performed in the framework of the KP-GT "Water and Related Chemistry in the Solar System", also known as "*Herschel* Solar System observations" (Hartogh et al. 2010).

Table 1. Summary of observations.

Obs. ID	Start time [UTC]	T_{obs} [min.]	Range^a [μm]
1342186536	30-Oct.-2009 00:58:36	116	51–72^k, 102–145^n
1342186537	30-Oct.-2009 03:01:48	133	51–62^l, 150–186^n
1342186538	30-Oct.-2009 05:22:32	203	60–73^l, 180–220^n
1342186539	30-Oct.-2009 08:53:20	151	68–85^m, 120–171^n
1342186540	30-Oct.-2009 11:31:41	236	82–102^m, 165-220^n
1342186571	31-Oct.-2009 14:35:00	82	118.4–120.9^n

Notes. $^{(a)}$ Grating order and filter: k = 2A, l = 3A, m = 2B, n = 1 red.

2. *Herschel*-PACS observations

All observations (Table 1) were carried out in chopped-nodded PACS range spectroscopy modes (2010) at high spectral sampling density. The entire spectral range of PACS has been measured at full instrumental resolution $\lambda/\delta\lambda$ ranging from 950 to 5500 depending on wavelength and grating order (2010). A summary of the observations is given in Table 1. Since blue and

⋆ *Herschel* is an ESA space observatory with science instruments provided by European-led Principal Investigator consortia and with important participation from NASA.

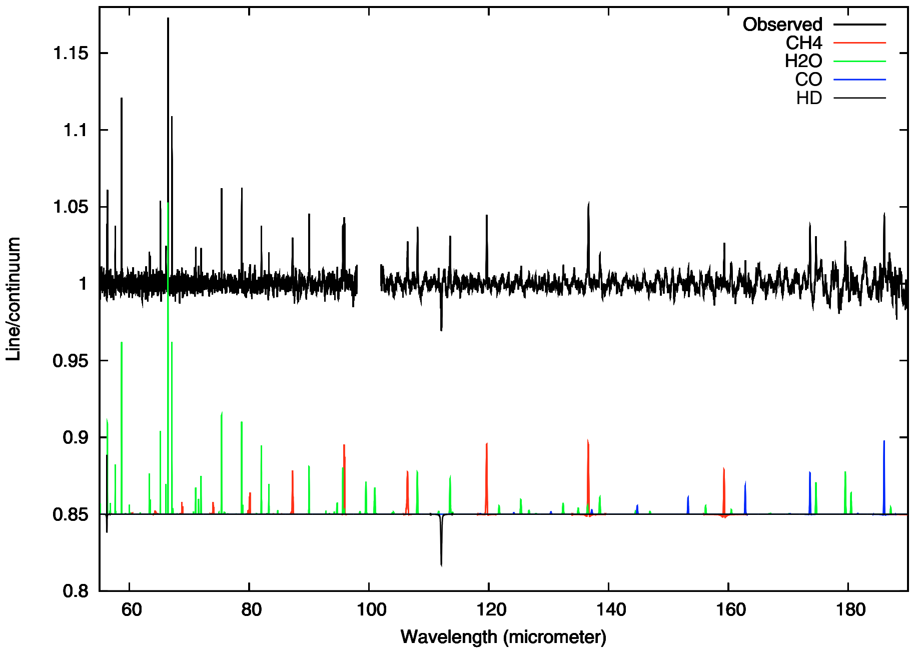

Fig. 1. Composite PACS spectrum of Neptune, expressed in line/local continuum ratios. For spectral ranges covered more than once (Table 1), the observation with the highest resolution has been selected. The region beyond 190 μm is not shown, owing to severe mixing of spectrometer orders. The bottom curves are synthetic spectra at appropriate spectral resolution that show the contributions of CH_4, H_2O, CO, and HD lines.

red spectrometer data are acquired in parallel, several spectral ranges have been observed in overlap. Given the instrumental spatial pixel size of 9.4″ × 9.4″, Neptune (2.297″ as seen from *Herschel*) can be considered as a point source, and the analyzed spectra therefore originate only in the central spatial pixel of the integral field spectrometer.

Starting from Level 0 products, the processing of all observations was carried by standard PACS pipeline modules (2010) up to Level 1. Individual spectral pixels were then scaled onto their common mean in order to improve the removal of signal outliers caused by cosmic ray hits. After application of an iterative σ-clipping, adapted to the instrumental resolution, the remaining data were rebinned onto an oversampled wavelength grid to ensure conservation of spectral resolution. The absolute flux calibration of the instrument and improvements on the relative spectral response function are still in progress. Therefore the resulting spectrum was then divided by its continuum, to be robust against forthcoming calibration updates. The composite spectrum is shown in Fig. 1. It shows emission signatures due to CH_4, H_2O, CO, as well as the R(0) and R(1) lines of HD at 112 and 56 μm, seen respectively in absorption and emission. At this stage of the data reduction, features below ~0.5–1% contrast must be treated with caution. No new species are detected at this level.

A dedicated line-scan high S/N observation of the CH_4 119.6 μm rotational line was also acquired in order to get a high precision measure of the CH_4 stratospheric abundance.

3. Analysis and discussion

3.1. Thermal profile and D/H abundance

Observations were analyzed by means of a standard radiative transfer code, in which the outgoing radiance from Neptune was integrated over all emission angles. The effective spectral resolution as a function of wavelength was determined by fitting the widths of the H_2O lines, whose profile is purely instrumental. We initially considered thermal profiles inferred in previous work (Marten et al. 2005; Bézard et al. 1998; Fletcher et al. 2010, respectively from ground-based, ISO, and AKARI observations). Below about 0.5 bar, all of them follow the *Voyager* radio-occultation profile (Lindal 1992, see also Moses et al. 2005). Above this level, these profiles diverge significantly, showing excursions of ~5 K over 10–200 mbar, and even larger dispersion (~10–20 K) at lower pressures. Over 50–200 μm, Neptune's continuum is formed near the 500 mbar level (T_B ~ 59 K). The HD lines typically probe the 10–500 mbar range (peak contribution near 2 mbar at line center). Because they show a contrasted absorption/emission appearance and because HD is vertically well mixed, they provide a sensitive thermometer in this region. For HD, we used the same linestrengths as in Feuchtgruber et al. (1999). We found that the Fletcher et al. (2010) nominal profile (their Fig. 5) allowed a much better fit of the HD lines than the other two profiles, and achieved optimum fit for temperatures equal to 0.9 × Fletcher + 0.1 × Marten (Fig. 2). This gives 54.5 K at the tropopause, ~3 K higher than in Lindal (1992). Given Neptune's temperature field as inferred from *Voyager* measurements (Conrath et al. 1998), this is probably related to the high latitude (42°S) of the *Voyager* occultations. Based on mid-infrared measurements of ethane, Hammel et al. (2006) also found enhanced temperatures (but at sub-mbar

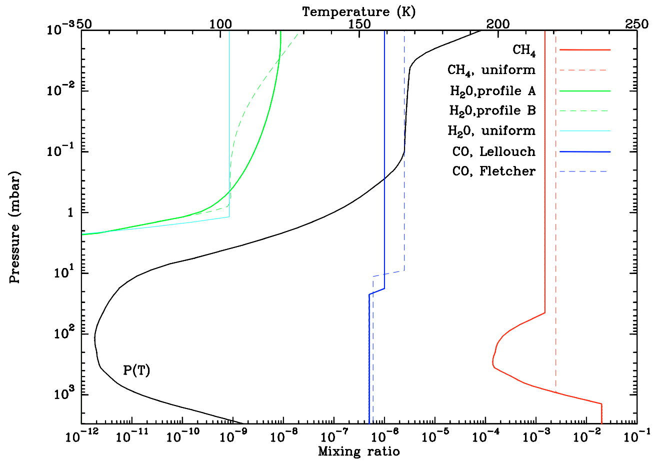

Fig. 2. Neptune's temperature and abundance profiles. CH_4 profiles condensing (thick red line) or not (thin red line) in the stratosphere are considered. For H_2O, profiles A and B are those of Feuchtgruber et al. (1997), multiplied by 0.95 and 0.9, respectively, and the "uniform" profile has a mixing ratio of 0.85 ppb above the condensation level. For CO, the profiles of Lellouch et al. (2005) and Fletcher et al. (2010) are shown. The black line shows the inferred temperature profile.

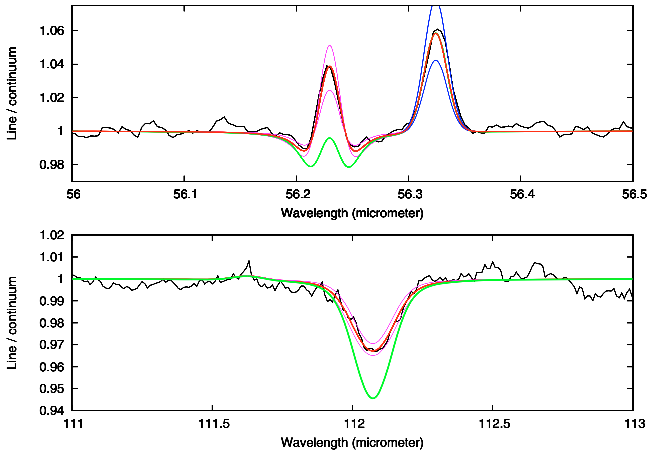

Fig. 3. Neptune's spectrum in the 56.0–56.5 and 111–113 μm ranges, showing HD lines at 56.25 μm (R(1)) and 112.1 μm (R(0)). Thick red line: model for HD/H_2 = 9×10^{-5} and the nominal thermal profile of Fig. 2. Thin pink lines: same for HD/H_2 = 6×10^{-5} and 12×10^{-5}. Green: model for $HD/H_2 = 9 \times 10^{-5}$ and Marten's et al. (2005) thermal profile). Note also the water line at 56.35 μm, well fitted by profile A in Fig. 2. The upper and lower blue lines show models for this H_2O profile multiplied and divided by 1.5.

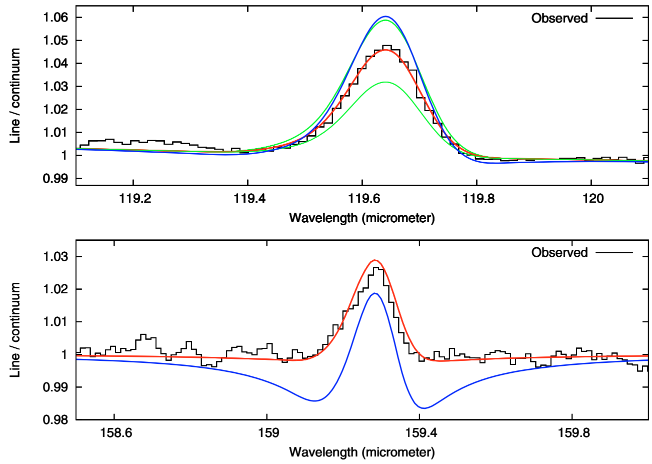

Fig. 4. Methane lines at 119.6 μm (Obs.ID 1342186571) and 159.3 μm (from Obs.ID 1342186537). Red: model for stratospheric q_{CH_4} = 0.0015 above the stratospheric saturation level (thick red line in Fig. 2). Green curves: same, but for q_{CH_4} = 0.0020 (upper curve) and 0.0010 (lower curve). Blue: model in which q_{CH_4} = 0.0025 down to ~800 mbar (thin red line in Fig. 2).

levels) compared to *Voyager*, a likely consequence of seasonal variability. Although the HD lines do not constrain temperatures above the 1 mbar level (needed in particular for analyzing the H_2O lines), we retained the 0.9 × Fletcher + 0.1 × Marten combination for all levels. We determined $HD/H_2 = (9 \pm 2) \times 10^{-5}$, i.e. a D/H ratio of $(4.5 \pm 1) \times 10^{-5}$ (Fig. 3). This is nominally less than but consistent with the $(6.5^{+2.5}_{-1.5}) \times 10^{-5}$ value inferred by Feuchtgruber et al. (1999) from observations of the R(2) line of HD by ISO/SWS, and confirms that Neptune is enriched in deuterium compared to the protosolar value ($\sim 2.1 \times 10^{-5}$) represented by Jupiter and Saturn (Lellouch et al. 2001). We defer a joint analysis of ISO and *Herschel* data to future work.

3.2. Methane, water, and carbon monoxide abundances and profiles

Methane has been observed in Neptune's stratosphere with a range of abundances exceeding the saturation value at the tropopause cold trap (e.g. Baines & Hammel 1994). The PACS spectrum shows several rotational lines of CH_4 in emission over 80–160 μm. Thanks to the mild temperature dependence of the Planck function in this spectral range, these lines are well suited to determination of the CH_4 stratospheric abundance. We assumed a CH_4 abundance of 2% in the deep troposphere, then following the saturation law. In the stratosphere, the CH_4 profile was characterized by its high-altitude mixing ratio (q_{CH_4}) and assumed to follow local saturation below the condensation point near 40 mbar. Utilizing the Boudon et al. (2010) results on the absolute CH_4 line strengths and in particular using the high S/N dedicated CH_4 120 μm line scan (Fig. 4), we determined $q_{CH_4} = (1.5 \pm 0.2) \times 10^{-3}$, consistent with Bézard et al. (1999b) ($(0.5–2) \times 10^{-3}$) but only marginally with Fletcher et al. (2010) ($(0.9 \pm 0.3) \times 10^{-3}$). Because of the progressive increase of the continuum level longwards of 100 μm, the CH_4 features at 137 μm and particularly 159 μm are sensitive to the CH_4 amount in the lower stratosphere. An alternate assumption would be that the CH_4 is supersaturated there, as could perhaps result from strong convective overshoot. This situation leads, however, to unobserved absorption wings at 159 μm and to inconsistent mixing ratios for the different lines (Fig. 4). A 1.5×10^{-3} mixing ratio is ~10 times greater than allowed by the 56 K cold trap, and consistent with saturation at 60 K. The most probable origin of this elevated stratospheric abundance is that CH_4 leaks from the hot (62–66 K at the tropopause) Southern region (Orton et al. 2007) and is redistributed planetwide by global circulation. A combined analysis of the PACS, ISO, *Spitzer*, and AKARI data in terms of stratospheric methane and temperature profile will be performed in the future.

The presence of H_2O in giant planet stratospheres, including Neptune's, was established from ISO/SWS 30–45 μm spectra (Feuchtgruber et al. 1997), demonstrating the existence of an external oxygen supply. In Neptune's case, ISO observations determined a $(2–4) \times 10^{14}$ cm^{-2} column density, but did not establish the water vertical profile, a parameter needed to derive the rate at which water is removed by vertical mixing and condensation and to infer the input flux of water. More than 20 H_2O lines, encompassing over a range in opacity of more than an order of magnitude (~0.2 to 2.5), are detected in the PACS spectrum. If uniformly mixed above the condensation level near 1.2 mbar, the water mixing ratio is $q_{H_2O} = (0.85 \pm 0.2)$ ppb, and its column density is $(2.1 \pm 0.5) \times 10^{14}$ cm^{-2}. Following Feuchtgruber et al. (1997), we also considered H_2O vertical profiles resulting from transport models, characterized by the eddy diffusion coefficient profile (profiles "A" and "B", see Fig. 2). For a given vertical profile, the water amounts we determined from the data were identical, to within 10%, to the values inferred from ISO. However, the associated external fluxes vary strongly (1.4×10^5 cm^{-2} s^{-1} for model A and 9×10^6 cm^{-2} s^{-1} for model B). We leave the detailed retrieval of Neptune's water profile (including PACS targeted observations of several weak lines and a deep 557 GHz HIFI observation) for the future. For the time being, an elementary analysis based on the integrated linewidths favors profile A over the other two water profiles (Fig. 5), suggesting that the water mixing ratio increases with altitude over 0.1–1 mbar.

Recent CO observations at millimeter/submillimeter wavelengths (Lellouch et al. 2005; Hesman et al. 2007) point to a higher abundance of CO in Neptune's stratosphere than in the troposphere. Both studies thus indicate a dual external/internal source, with the external source possibly provided by an ancient cometary impact. They also provide consistent values of the CO tropospheric mixing ratio (0.5–0.6 ppm). However, they differ by more than a factor of 2 (1×10^{-6} and 2.2×10^{-6}, respectively)

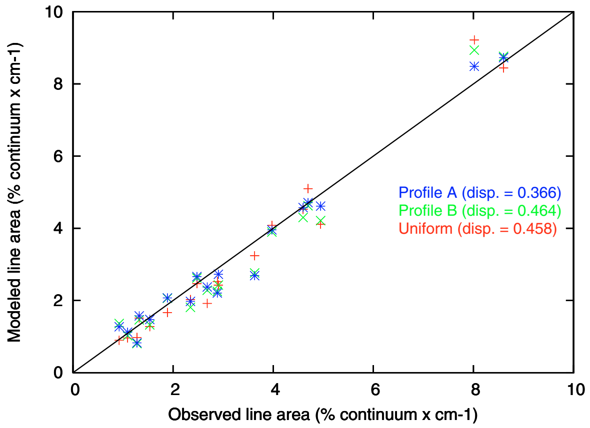

Fig. 5. Modeled vs. observed H_2O line integrated areas for the three water profiles of Fig. 2. Line areas are expressed in cm^{-1} ×% of the local continuum. For each profile, the mean rms dispersion (in the same unit) between observed and modeled areas is given. Profile A provides a better fit to the data than do the other two profiles.

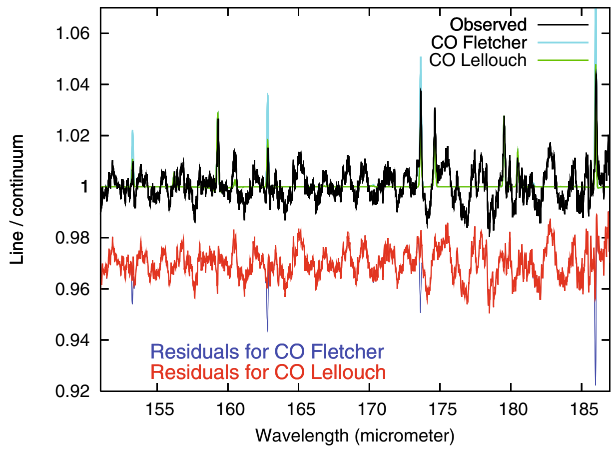

Fig. 6. CO lines at 153–187 μm, compared with models using the CO distributions of Lellouch et al. (2005) and Fletcher et al. (2010), shown in Fig. 2. CO lines occur at 154, 163, 174 and 186 μm. Other features are due to CH_4 and H_2O. The bottom curves are difference (observed – modeled) plots (shifted by 0.97), favoring the Lellouch et al. profile.

on the stratospheric CO abundance (Fig. 2). Support for the Hesman et al. value was reported from the detection of CO fluorescence at 4.7 μm by AKARI (Fletcher et al. 2010), from which a 2.5 ppm abundance of CO above the 10-mbar pressure level was inferred. We find here that the CO lines longward of 150 μm (Fig. 6) instead imply a CO stratospheric abundance of ~1 ppm, in agreement with Lellouch et al. (2005). The detailed determination of the CO profile will be possible from combined analysis of PACS, SPIRE, and new broadband ground-based millimeter data.

Acknowledgements. PACS has been developed by a consortium of institutes led by MPE (Germany) and including UVIE (Austria); KUL, CSL, IMEC (Belgium); CEA, OAMP (France); MPIA (Germany); IFSI, OAP/AOT, OAA/CAISMI, LENS, SISSA (Italy); IAC (Spain). This development has been supported by the funding agencies BMVIT (Austria), ESA-PRODEX (Belgium), CEA/CNES (France), DLR (Germany), ASI (Italy), and CICT/MCT (Spain). Additional funding support for some instrument activities has been provided by ESA. Data presented in this paper were analysed using "HIPE", a joint development by the *Herschel* Science Ground Segment Consortium, consisting of ESA, the NASA *Herschel* Science Center, and the HIFI, PACS and SPIRE consortia.
We are indebted to Bruno Bézard for important discussions on the HD and CH_4 line parameters.

References

Baines, K., & Hammel, H. 1994, Icarus, 109, 20
Bézard, B., Encrenaz, T., Lellouch, E., Feuchtgruber, H. 1998, Science, 283, 800
Bézard, B., Romani, P., Feuchtgruber, H., & Encrenaz, T. 1999a, ApJ, 515, 868
Bézard, B., Encrenaz, T., & Feuchtgruber, H. 1999b, ESA-SP 427, 153
Boudon, V., et al. 2010, J. Quant. Spectro. Rad. Transf., 111, 1117
Burgdorf, M., Orton, G. S., Davis, G. R., et al. 2003, Icarus, 164, 244
Conrath, B. J., Gierasch, P. J., & Ustinov, E. A. 1998, Icarus, 135, 501
Feuchtgruber, H., Lellouch, E., de Graauw, T., et al. 1997, Nature, 389, 159
Feuchtgruber, H., Lellouch, E., Bézard, B., et al. 1999, A&A, 341, L17
Fletcher, L. N., Drossart, P., Burgdorf, M., et al. 2010, A&A, 514, A17
Hammel, H. B., Lynch, D. K., Russell, R. W., et al. 2006, ApJ, 644, 1326
Hartogh, P., Lellouch, E., et al. 2009, Planet. Space Sci., 57, 1596
Hesman, B. E., Davis, G. R., et al. 2007, Icarus, 186, 342
Lellouch, E., Bézard, B., Fouchet, T., et al. 2001, A&A, 370, 610
Lellouch, E., Moreno, & G. Paubert, 2005, A&A, 430, L37
Lindal, G. F. 1992, AJ, 103, 967
Marten, A., et al. 2005, A&A, 437, 319
Meadows, V. S., et al. 1999, Icarus, 197, 585
Moses, J. I., et al. 2005, JGR, 110, E08001
Orton, G. S., Encrenaz, T., Leyrat, C., et al. 2007, A&A, 473, L5
Pilbratt, G. L., et al. 2010, A&A, 518, L1
Poglitsch, A., Waelkens, C., Geis, N., et al. 2010, A&A, 518, L2
PACS Observers Manual 2010,
http://Herschel.esac.esa.int/Docs/PACS/pdf/pacs_om.pdf

[1] LESIA, Observatoire de Paris, 5 place Jules Janssen, 92195 Meudon, France
e-mail: emmanuel.lellouch@obspm.fr
[2] Max-Planck-Institut für Sonnensystemforschung, Katlenburg-Lindau, Germany
[3] Max-Planck-Institut für extraterrestrische Physik, Giessenbachstraße, 85748 Garching, Germany
[4] Instituut voor Sterrenkunde, Katholieke Universiteit Leuven, Belgium
[5] SRON, Groningen, The Netherlands
[6] JPL, California Institute of Technology, Pasadena, USA
[7] Space Research Centre, Polish Academy of Science, Warszawa, Poland
[8] Blue Sky Spectroscopy Inc., Lethbridge, Alberta, Canada
[9] European Space Astronomy Center, Madrid, Spain
[10] Instituto de Astrofísica de Andalucía (CSIC), Granada, Spain
[11] California Institute of Technology, Pasadena, USA
[12] Rutherford Appleton Laboratory, Oxfordshire, U K
[13] Deutsches Zentrum für Luft- und Raumfahrt (DLR), Bonn, Germany
[14] University of Michigan, Ann Arbor, USA
[15] Université de Bordeaux, Observatoire Aquitain des Sciences de l'Univers, CNRS, UMR 5804, Laboratoire d'Astrophysique de Bordeaux, France
[16] Laboratorio de Astrofísica Molecular, CAB. INTA-CSIC, Spain
[17] Joint Astronomy Center, Hilo, USA
[18] LERMA, Observatoire de Paris, and Univ. Pierre et Marie Curie, Paris, France
[19] F.R.S.-FNRS, Institut d'Astrophysique et de Géophysique, Liège, Belgium
[20] Herschel Science Centre, ESA Centre, Madrid, Spain
[21] University of Lethbridge, Canada
[22] University of Bern, Switzerland
[23] University of Cologne, Germany
[24] Max-Planck-Institut für Radioastronomie, Bonn, Germany
[25] Experimental Physics Dept., National University of Ireland Maynooth, Co. Kildare. Ireland